Hot-electron magneto-miniband transport in lateral semiconductor superlattices

1993 J. Phys.: Condens. Matter 5 8579

(http://iopscience.iop.org/0953-8984/5/45/010)

J. Phys.: Condens. Matter 5 (1993) 8579–8586. Printed in the UK

Hot-electron magneto-miniband transport in lateral semiconductor superlattices

X L Lei

China Centre of Advanced Science and Technology (World Laboratory), PO Box 8730, Beijing 100080, People's Republic of China
State Key Laboratory of Functional Materials for Informatics, Shanghai Institute of Metallurgy, Chinese Academy of Sciences, 865 Changning Road, Shanghai 200050, People's Republic of China

Received 27 July 1993

Abstract. We present a theoretical analysis of hot-electron magneto-miniband transport in a lateral semiconductor superlattice. Our approach is based on the recently developed balance-equation theory extended to the lateral superlattice in the presence of crossed magnetic and electric fields. Realistic scatterings due to impurities, acoustic phonons and polar optic phonons are taken into account in the study. Negative differential velocities appear at high electric field for all the directions in the superlattice plane, but the linear mobility and the peak drift velocity in the ⟨10⟩-direction are higher than those in the ⟨11⟩-direction. Special attention is paid to the perpendicular (Hall) conduction. The magnitude and the sign of the Hall resistivity in linear and non-linear transport not only varies strongly with the carrier density but also varies with the electron temperature.

1. Introduction

With the technological advances in semiconductor microfabrication, the lateral semiconductor superlattice (LSSL), a quasi-two-dimensional electron system spatially modulated by a two-dimensional periodic potential, has become a subject of intense experimental and theoretical investigations [1–5]. Most of the recent studies have concentrated on the low-temperature properties of the LSSL prepared on a high-mobility two-dimensional electron gas having weak or moderate modulation potential and with a lattice constant of a few hundred nanometres, which exhibits transport properties directly due to the density of states and other structures resulting from the interplay between the magnetic field and the modulation potential. Nevertheless, systems with smaller lattice constant and larger modulation potential, proposed earlier [1], are also of great interest. Such a structure is a two-dimensional version of the Esaki–Tsu superlattice [6], in which the band-conduction mechanism dominates and impurity and phonon scatterings play an important role. Negative differential velocity of Esaki–Tsu origin has recently been extensively studied both experimentally and theoretically [7–12]. Under the influence of a strong electric field carriers become hot and oscillations related to the structure of the density of states and the Landau quantization are smeared. Such an LSSL is potentially a good candidate for use in the microwave oscillator [10–11], since its miniband conduction may exhibit negative differential mobility in any direction of the current flow in the plane and a perpendicular applied magnetic field offers an additional means to tune the velocity–field behaviour.

The purpose of the present paper is to give a systematic investigation of hot-electron magneto-miniband transport in the LSSL using the balance equation approach [12–14] extended to the LSSL in the presence of crossed magnetic and electric fields.

0953-8984/93/458579+08$07.50

2. Model and balance equations

As a model of a strongly modulated LSSL we consider a quasi-two-dimensional GaAs base layer of thickness d_z in the z direction. There is a square two-dimensional (2D) superlattice potential of lattice constant d applied in the x and y directions, resulting in 2D minibands in the electron energy spectrum. In the limit of strong modulation potential these minibands are essentially the tight-binding type. We consider only the lowest miniband and thus write the electron energy in the form

$$\varepsilon_n(k_\parallel) = \varepsilon_n + \varepsilon(k_x) + \varepsilon(k_y) \tag{1}$$

with

$$\varepsilon(k) \equiv (\Delta/2)(1 - \cos kd) \tag{2}$$

where $k_\parallel \equiv (k_x, k_y)$ denotes the in-plane wavevector of the 2D superlattice, $-\pi/d < k_x \leqslant \pi/d$, $-\pi/d < k_y \leqslant \pi/d$, and 2Δ is the bandwidth of this 2D miniband. ε_n $(n = 1, 2, ...)$ represent the quantized energy levels in the z direction due to the vertical confinement d_z.

In the presence of an electric field in the x–y plane, $\boldsymbol{E} = (E_x, E_y, 0)$, and a magnetic field in the z direction, $\boldsymbol{B} = (0, 0, B)$, the effective Hamiltonian related to the in-plane movement of N interacting electrons in this LSSL can be written as

$$H_e = \sum_j h_j + H_{ee} \tag{3}$$

with

$$h_j = \varepsilon(p_{xj}) + \varepsilon(p_{yj} - eBx_j) - ex_jE_x - ey_jE_y \tag{4}$$

where e is the electron charge, p_{xj}, p_{yj} and x_j ,y_j represent the momentum and position operators of the jth electron, and H_{ee} stands for the carrier–carrier interaction. We have chosen the vector potential as $\boldsymbol{A} = (0, Bx, 0)$.

Following the balance equation approach [12–14], we assume that the strong intercarrier interaction promotes rapid thermalization of carriers in the reference frame in which the total momentum of the carriers vanishes. This enables us to characterize the transport state of this many-carrier system by an in-plane average momentum per carrier, $p_d = (p_x, p_y)$, and an electron temperature T_e. The introduction of these two parameters, which are included in the initial state, facilitates solving the Liouville equation to obtain the density matrix. Acceleration- and energy-balance equations are derived by identifying the rate of change of the drift velocity $v_d = (v_x, v_y, 0)$ to be the average of the operator $\sum_j [[H, r_j], H]/N$, and the rate of change of the electron energy (per carrier) h_e to be the average of $i[H, H_e]/N$, yielding

$$dv_x/dt = eE_x/m_x^* + \left(eBv_y/m_x^*\right)\gamma + A_{ix} + A_{px} \tag{5}$$

$$dv_y/dt = eE_y/m_y^* - \left(eBv_x/m_y^*\right)\gamma + A_{iy} + A_{py} \tag{6}$$

$$dh_e/dt = eE_xv_x + eE_yv_y - W \tag{7}$$

Here $A_{i\alpha}$ and $A_{p\alpha}$ $(\alpha = x, y)$ are the frictional accelerations due to impurities and due to phonons in the α direction, and are given by

$$A_{i\alpha} = \frac{2\pi n_I}{N} \sum_{m,n,k_\parallel,q} |u(q)|^2 |J_{n,m}(q_z)|^2 |g(q_\parallel)|^2 \left[v(k_\alpha + q_\alpha) - v(k_\alpha)\right]$$

$$\times \delta\left[\varepsilon_n(k_\parallel + q_\parallel) - \varepsilon_m(k_\parallel)\right] \frac{f[\bar{\varepsilon}_m(k_\parallel), T_e] - f[\bar{\varepsilon}_n(k_\parallel + q_\parallel), T_e]}{\left|\epsilon[q, \bar{\varepsilon}_m(k_\parallel) - \bar{\varepsilon}_n(k_\parallel + q_\parallel)]\right|^2} \tag{8}$$

$$A_{p\alpha} = \frac{4\pi}{N}\sum_{m,n,k_\parallel,q,\lambda}|M(q,\lambda)|^2|J_{m,n}(q_z)|^2|g(q_\parallel)|^2\left[v(k_\alpha+q_\alpha)-v(k_\alpha)\right]$$
$$\times\delta\left[\varepsilon_n(k_\parallel+q_\parallel)-\varepsilon_m(k_\parallel)+\Omega_{q,\lambda}\right]\frac{f[\bar{\varepsilon}_m(k_\parallel),T_e]-f[\bar{\varepsilon}_n(k_\parallel+q_\parallel),T_e]}{\left|\epsilon[q,\bar{\varepsilon}_m(k_\parallel)-\bar{\varepsilon}_n(k_\parallel+q_\parallel)]\right|^2}$$
$$\times\left[n\left(\frac{\Omega_{q,\lambda}}{T}\right)-n\left(\frac{\bar{\varepsilon}_m(k_\parallel)-\bar{\varepsilon}_n(k_\parallel+q_\parallel)}{T_e}\right)\right] \tag{9}$$

and W is the energy-loss rate per carrier from the electron system to the phonon system

$$W = \frac{4\pi}{N}\sum_{m,n,k_\parallel,q,\lambda}|M(q,\lambda)|^2|J_{m,n}(q_z)|^2|g(q_\parallel)|^2\Omega_{q,\lambda}\left[v(k_\alpha+q_\alpha)-v(k_\alpha)\right]$$
$$\times\delta\left[\varepsilon_n(k_\parallel+q_\parallel)-\varepsilon_m(k_\parallel)+\Omega_{q,\lambda}\right]\frac{f[\bar{\varepsilon}_m(k_\parallel),T_e]-f[\bar{\varepsilon}_n(k_\parallel+q_\parallel),T_e]}{\left|\epsilon[q,\bar{\varepsilon}_m(k_\parallel)-\bar{\varepsilon}_n(k_\parallel+q_\parallel)]\right|^2}$$
$$\times\left[n\left(\frac{\Omega_{q,\lambda}}{T}\right)-n\left(\frac{\bar{\varepsilon}_m(k_\parallel)-\bar{\varepsilon}_n(k_\parallel+q_\parallel)}{T_e}\right)\right]. \tag{10}$$

In deriving the above equations we have assumed that phonons are three-dimensional (3D) bulk modes and that impurities are 3D randomly distributed. In the above expressions $\bar{\varepsilon}_n(k_\parallel)\equiv\varepsilon_n(k_\parallel-p_d)$ is the relative electron energy, $v(k_\alpha)\equiv\partial\varepsilon(k_\parallel)/\partial k_\alpha = v_m\sin k_\alpha d$ is the velocity function in the α direction with $v_m\equiv\Delta d/2$; $u(q)$ and n_I represent the impurity potential and the impurity density, $M(q,\lambda)$ is the electron–phonon matrix element for phonons of wavevector q in branch λ, having frequency $\Omega_{q,\lambda}$; $n(x)=(\exp x-1)^{-1}$ is the Bose function, $\epsilon(q,\omega)$ is the dielectric function of the carriers in the random-phase approximation; $J_{m,n}(q_z)$ is a form factor determined by the confined wavefunction in the z direction and $g(q_\parallel)$ is a form factor associated with the lowest 2D miniband wavefunction.

The drift velocities v_x and v_y, and the ensemble averaged inverse effective mass $1/m_x^*$ and $1/m_y^*$, are given by

$$v_x = v_m\alpha(T_e)\sin p_x d \tag{11}$$
$$v_y = v_m\alpha(T_e)\sin p_y d \tag{12}$$
$$1/m_x^* = (1/M^*)\alpha(T_e)\cos p_x d \tag{13}$$
$$1/m_y^* = (1/M^*)\alpha(T_e)\cos p_y d \tag{14}$$

with $1/M^*\equiv\Delta d^2/2$. The quantities $\alpha(T_e)$ and γ are defined by

$$\alpha(T_e) = \frac{2}{N}\sum_{n,k_\parallel}\cos(k_x d)\,f\left[\varepsilon_n(k_\parallel),\,T_e\right] \tag{15}$$

$$\gamma = \frac{2}{N\alpha(T_e)^2}\sum_{n,k_\parallel}\cos(k_x d)\,\cos(k_y d)\,f\left[\varepsilon_n(k_\parallel),\,T_e\right]. \tag{16}$$

In these equations

$$f\left[\varepsilon_n(k_\parallel),T_e\right] = 1/\left\{\exp[(\varepsilon_n(k_\parallel)-\mu)/T_e]+1\right\} \tag{17}$$

is the Fermi distribution function, and the chemical potential μ is determined by the condition that the total number of carriers is equal to N:

$$N = 2\sum_{n,k_\parallel}f\left[\varepsilon_n(k_\parallel),\,T_e\right] \tag{18}$$

3. Hall resistivity

Assume that the drift momentum p_d, thus the drift velocity v_d, is along the x direction: $p_d = (p_x, 0, 0)$, $v_d = (v_d, 0, 0)$. The steady-state acceleration- and energy-balance equations are reduced to

$$eE_x/m_x^* + A_{ix} + A_{px} = 0 \tag{19}$$

$$eE_y/m_y^* - (eBv_d/m_y^*)\gamma = 0 \tag{20}$$

$$eE_x v_d - W = 0. \tag{21}$$

The sheet current density (in the x direction) is given by

$$J_x = N_s e v_d. \tag{22}$$

Defining the (non-linear) longitudinal sheet resistivity as $\rho_{xx} \equiv E_x/J_x$, we have from equation (19)

$$\rho_{long} = \rho_{xx} = -m_x^*(A_{ix} + A_{px})/N_s e^2 v_d. \tag{23}$$

On the other hand, the electric field along the y direction is determined by equation (20):

$$E_y = Bv_d\gamma. \tag{24}$$

This yields the transverse (Hall) resistivity

$$\rho_{trans} = \rho_{yx} \equiv E_y/J_x = (\gamma/N_s e)B \tag{25}$$

and the Hall coefficient

$$R_H = \gamma/N_s e = (\gamma/N_s d^2)(d^2/e). \tag{26}$$

Note that the longitudinal resistivity ρ_{long} obviously depends on the current direction, due to the anisotropic 2D energy band. Nevertheless, the expressions for the transverse resistivity ρ_{trans} and for the Hall coefficient R_H, equations (25) and (26), are universal, independent of the direction of the current flow in the plane.

In the case of a parabolic band (free electron) the Hall coefficient is given by a well known expression

$$R_H = 1/N_s e \tag{27}$$

which is the same in linear (weak-electric field) and non-linear (strong-electric field) transport [15], as long as the electron density remains unchanged.

The effect of the energy-band non-parabolicity is fully contained in the coefficient γ. Depending on the degree of non-parabolicity of the energy band, both the magnitude and the sign of the coefficient γ may change on changing the electron density N_s. To see the meaning of this γ–N_s variation we consider the energy band given by equations (1) and (2) with fixed 3-direction energy level (a typical 2D tight-binding band) at zero temperature. The maximum two electrons per unit cell can be contained in this band, i.e. the density of electrons that fills up the whole band is $N_s d^2 = 2$. In the vicinity of the band bottom, i.e. $N_s d^2 \ll 1$, the zero-temperature Fermi level ε_F (the band bottom is chosen as the energy zero) is

$$\varepsilon_F/\Delta \simeq (\pi/2)N_s d^2 \tag{28}$$

and the coefficient

$$\gamma \simeq 1. \tag{29}$$

The Hall coefficient $R_H \simeq 1/N_s e$. This is a natural result: near the bottom the band is essentially parabolic and is occupied by electrons of density N_s. On the other hand, in the vicinity of the band top, i.e. $1 - N_s d^2/2 \ll 1$, the zero-temperature Fermi level is given by

$$\varepsilon_F/\Delta \simeq 2 - \pi\left(1 - N_s d^2/2\right) \tag{30}$$

and

$$\gamma \simeq \left(N_s d^2/2\right)\left(1 - N_s d^2/2\right)^{-1}. \tag{31}$$

The Hall coefficient is

$$R_H = \gamma/N_s e = -1/N_s^* e \tag{32}$$

with the effective density

$$N_s^* = (2/d^2 - N_s). \tag{33}$$

This is equivalent to a case of parabolic band occupied by carriers having charge $-e$ and density N_s^* given by equation (33). This N_s^* is just the number density of the states unoccupied by electrons in the 2D band.

The expression for the Hall coefficient, equation (26), could be interpreted as that of effective carriers, having an effective density of N_s/γ and carrying charge of $\mathrm{sgn}(\gamma)e$.

The calculated γ as a function of electron density, $N_s d^2$, is plotted in figure 1, together with $\gamma/N_s d^2$. The transition from the electron-type conduction to the hole-type conduction appears naturally. Carriers are electron like when the electron occupation is less than half filled ($N_s d^2 < 1$), and are hole like when the electron occupation exceeds half filled ($N_s d^2 > 1$). The effective carrier number density diverges at both sides of the half-filled electron occupation ($N_s d^2 = 1$).

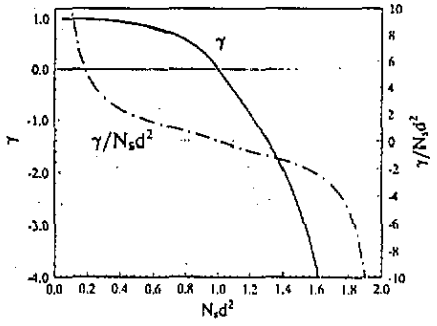

Figure 1. Zero-temperature coefficient γ (equation (16)) and $\gamma/N_s d^2$ (see equation (26)) are shown as functions of the band occupation $N_s d^2$ for a 2D tight-binding system.

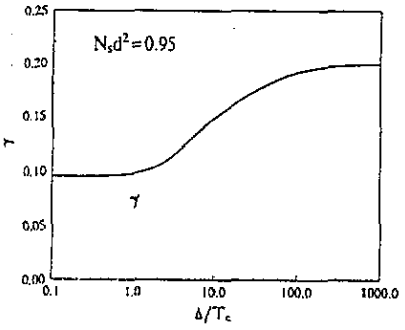

Figure 2. Temperature dependence of the coefficient γ in a 2D tight-binding system with $N_s d^2 = 0.95$.

To see the temperature dependence of the Hall resistivity we show in figure 2 the calculated γ against Δ/T_e for $N_s d^2 = 0.95$. This weak temperature dependence of γ indicates that in a non-parabolic band, the strong electric field may slightly show up in the Hall resistivity through its effect on the electron temperature, but the effect is generally quite small.

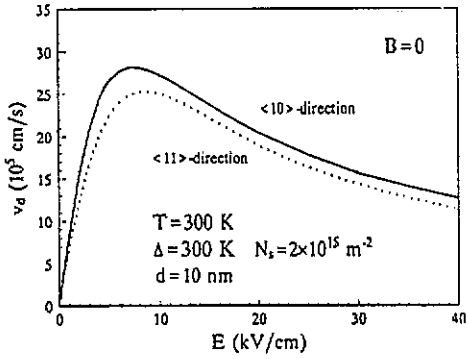

Figure 3. Drift velocity versus electric field for ⟨10⟩ and ⟨11⟩ directions in a lateral superlattice of Δ = 300 K, d = 10 nm, N_s = 2.0×10^{11} cm^2, d_z= 10 nm, and low-temperature x direction linear mobility $\mu(0)$ = 1.0 m^2 V^{-1} s^{-1}, in the absence of magnetic field at lattice temperature T = 30K.

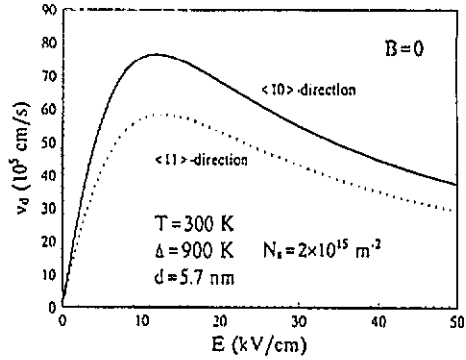

Figure 4. Drift velocity versus electric field for ⟨10⟩ and ⟨11⟩ directions in a lateral superlattice of Δ = 900 K, d = 5.7 nm, N_s = 2.0 × 10^{11} cm^2, d_z = 10 nm, and low-temperature x direction linear mobility $\mu(0)$ = 1.0 m^2 V^{-1} s^{-1}, in the absence of magnetic field at lattice temperature T = 300 K.

4. Negative differential mobility

Balance equations (5)–(7) determine the steady-state and time-dependent transport in an LSSL under the influence of a uniform electric field in any direction in the x–y plane and a uniform magnetic field in the z direction. The steady-state non-linear longitudinal conductions have been calculated for the applied electric field along ⟨10⟩ and ⟨11⟩ directions in two different lateral GaAs-base superlattices at lattice temperature T = 300 K without a magnetic field (B = 0). In this we have included impurity, acoustic-phonon (through the deformation potential and piezoelectric couplings with electrons) and polar-optic-phonon (through the Fröhlich coupling with electrons) scatterings in the calculation. The vertical extension d_z is assumed to be 10 nm for both systems, and thus taking the lowest z direction subband is good enough for the present calculation. The calculated drift velocities v_d and the electron temperature T_e as functions of the electric field E applied along the ⟨10⟩ and ⟨11⟩ directions are shown in figures 3 and 4 respectively for an LSSL of d = 10 nm, Δ = 300 K and for an LSSL of d = 5.7 nm, Δ = 90 K. We assume that the carrier sheet density $N_s = 2.0 \times 10^{11}$ cm^{-2}, the z extension d_z = 10 nm, and the low-temperature linear mobility along the x direction $\mu(0)$ = 1.0 m^2 V^{-1} s^{-1}. Negative differential mobilities appear in both directions. We find that although low-electric-field (linear) mobilities are the same for both directions, the non-linear drift velocity in the ⟨10⟩ direction is higher than that in the ⟨11⟩ direction for a given strength of the electric field for both samples in this carrier density. This is at variance with the earlier Monte Carlo calculation [1].

5. Non-linear magneto-transport

The application of a magnetic field in the z direction has a significant influence on the non-linear drift velocity as a function of the electric field. To see this we show in figure 5 the drift velocity v_d versus the electric field E applied along the x direction at lattice temperature T = 300 K for an LSSL having Δ = 300 K, d = 10 nm, $N_s = 2.0 \times 10^{11}$ cm^2, d_z = 10 nm, and low-temperature linear mobility $\mu(0)$ = 1.0 m^2 V^{-1} s^{-1}, without and with a

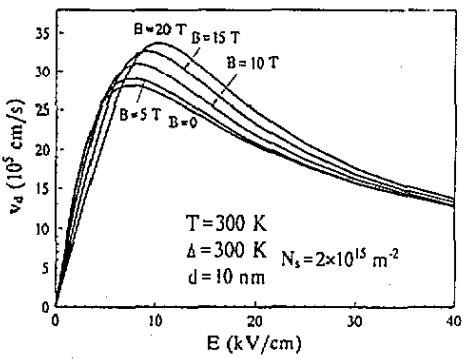

Figure 5. Drift velocity v_d is plotted as a function of the electric field E applied in the x direction in the presence of magnetic fields of strengths B = 0, 5, 10, 15 and 20 T, for a lateral superlattice of Δ = 300 K, d = 10 nm, $N_s = 2.0 \times 10^{11}$ cm^2, d_z = 10 nm, and low-temperature linear mobility $\mu(0)$ = 1.0 m^2 V^{-1} s^{-1} at lattice temperature T = 300 K.

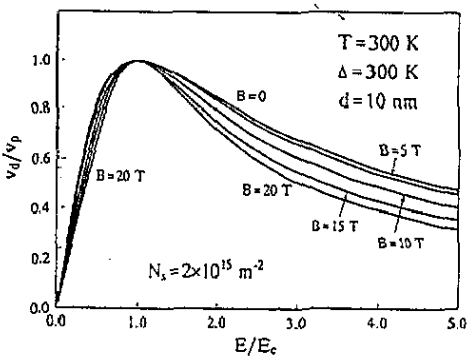

Figure 6. Normalized drift velocity v_d/v_p versus normalized electric field E/E_c for the same set of data as shown in figure 5.

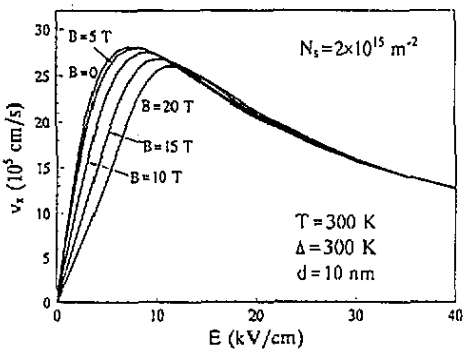

Figure 7. The x component of the drift velocity v_x is plotted as a function of the electric field E applied in the x direction in the presence of magnetic fields having strengths B = 0, 5, 10, 15 and 20 T, for a lateral superlattice of Δ = 300 K, d = 10 nm, $N_s = 2.0 \times 10^{11}$ cm^2, d_z = 10 nm, and low-temperature linear mobility $\mu(0)$ = 1.0 m^2 V^{-1} s^{-1} at lattice temperature T = 300 K.

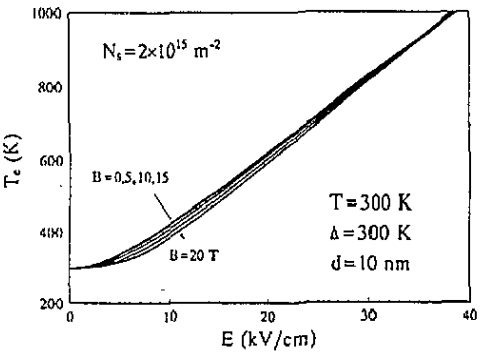

Figure 8. Electron temperature T_e is shown as a function of the electric field E applied in the x direction in the presence of magnetic fields having strengths B = 0, 5, 10, 15 and 20 T, for a lateral superlattice of Δ = 300 K, d = 10 nm, $N_s = 2.0 \times 10^{11}$ cm^2, d_z = 10 nm, and low-temperature linear mobility $\mu(0)$ = 1.0 m^2 V^{-1} s^{-1} at lattice temperature T = 300 K.

magnetic field of strength B = 0, 5, 10, 15, and 20 T in the z direction. The magnetic field significantly affects the drift velocity behaviour at low and medium strengths of the electric field: it increases the peak drift velocity v_p and shifts the threshold electric field E_c towards higher strength. At very high electric field the influence of the magnetic field diminishes. Therefore the LSSL exhibits a steeper negative differential velocity in the presence of a magnetic field. This enhancement of the negative differential mobility is more clearly seen in figure 6, where the drift velocity normalized by its peak value v_p is plotted as a function of the electric field normalized by the threshold field E_c for the same set of data as shown in figure 5. Note that in the presence of a magnetic field ($B \neq 0$) the drift velocity deviates

from the electric field direction (x direction). If we plot the x direction drift velocity v_x as a function of the electric field E, we have the results shown in figure 7. The application of a magnetic field always reduces the electron temperature at given applied electric field, as is shown in figure 8.

6. Summary

We have investigated the linear and non-linear magneto-miniband transport in LSSL of strong modulation potential. The system is modelled by a z-direction confined two-dimensional tight-binding structure. Our study is based on the balance-equation theory for miniband transport extended to an LSSL in the presence of crossed magnetic and electric fields. The LSSL exhibits negative differential mobility comparable to that in an Esaki–Tsu superlattice in all directions of the electric fields in the plane. A magnetic field applied perpendicular to the plane reduces the electron temperature and offers a way to tune the drift-velocity–field behaviour.

Acknowledgment

The author wishes to thank Professor C S Ting for helpful discussions. This work was supported by the National Natural Science Foundation of China.

References

[1] Reich R K, Grodin R O and Ferry D K 1983 *Phys. Rev.* B **27** 3483
[2] Lorke A 1992 *Surf. Sci.* **263** 307
[3] Weiss D, Menschig A, von Klitzing K and Weimann G 1992 *Surf. Sci.* **263** 314
[4] Gerhardts P R, Weiss D and Wulf U 1991 *Phys. Rev.* B **43** 5192
[5] Pfannkuche D and Gerhardts P R 1992 *Phys. Rev.* B **46** 12606
[6] Esaki L and Tsu R 1970 *IBM J. Res. Dev.* **14** 61
[7] Sibille A, Palmier J F, Wang H and Mollot F 1990 *Phys. Rev. Lett.* **64** 52
[8] Beltram F, Capasso F, Sivco D L, Hutchinson A L and Chu S N G 1990 *Phys. Rev. Lett.* **64** 3167
[9] Grahn H T, von Klitzing K, Ploog K and Döhler G H 1991 *Phys. Rev.* B **43** 12094
[10] Hadjazi M, Sibille A, Palmier P J and Mollot F 1992 *Electron. Lett.* **27** 1101
[11] Lei X L, Horing N J M, Cui H L and Thomber K K 1993 *Phys. Rev.* B **48** 5366; 1993 *Solid State Commun.* **86** 231
[12] Lei X L, Horing N J M and Cui H L 1991 *Phys. Rev. Lett.* **66** 3277; 1991 *J. Phys.: Condens. Matter* **4** 9375
[13] Lei X L and Ting C S 1984 *Phys. Rev.* B **30** 4809; 1985 *Phys. Rev.* B **32** 1112
[14] Lei X L 1992 *Phys. Status Solidi* b **170** 519
[15] Lei X L, Cai W and Ting C S 1985 *J. Phys. C: Solid State Phys.* **18** 4315